Surface morphology of crystalline antimony islands on graphite at room temperature

2006 J. Phys.: Condens. Matter 18 3425

(http://iopscience.iop.org/0953-8984/18/13/010)

INSTITUTE OF PHYSICS PUBLISHING JOURNAL OF PHYSICS: CONDENSED MATTER

J. Phys.: Condens. Matter **18** (2006) 3425–3434 doi:10.1088/0953-8984/18/13/010

Surface morphology of crystalline antimony islands on graphite at room temperature

S S Kushvaha[1], Z Yan[1,2], W Xiao[1] and X-S Wang[1]

[1] Department of Physics, National University of Singapore, 2 Science Drive 3, 117542, Singapore
[2] Department of Physics, Lanzhou University, Lanzhou, People's Republic of China

E-mail: phywxs@nus.edu.sg (X-S Wang)

Received 15 December 2005
Published 14 March 2006
Online at stacks.iop.org/JPhysCM/18/3425

Abstract

Antimony islands of different shapes and dimensions were grown on highly oriented pyrolytic graphite (HOPG) at room temperature in ultrahigh vacuum. Three-dimensional (3D) spherical, 2D thin films and 1D nanorods of Sb on graphite were studied using *in situ* scanning tunnelling microscopy. Sb was evaporated in the form of Sb_4, which interacts with HOPG weakly and exhibits a high surface mobility, resulting in preferential nucleation of 3D spherical islands at defect sites. Surface diffusion and aggregation lead to the formation of nanoparticles with various shapes and sizes. The shape and size of islands depend on growth parameters, i.e. flux and deposition time. The 3D and 2D structures of Sb on graphite have the same bulk crystalline rhombohedral (α-Sb) structure, but the 1D nanorods show a highly compressed structure different from the α-Sb lattice.

1. Introduction

In nanotechnology, nanoparticles are important due to their physical and chemical properties which can be rather different from those of bulk materials. The study of the growth of nanostructures and thin films on different substrates has let us discover new methods for the synthesis of new materials with interesting properties. In many cases, the interaction between over-layer and substrate is very strong so the structures grown are far from the 'free-standing' state [1, 2]. However, studies of nanostructures on inert substrates have attracted significant attention in recent years, since nearly free-standing nanostructures can be formed on such substrates. These types of nanostructures can be used as catalysts [3, 4], quantum dots [5], and single-domain magnets [6], among others. Inert substrates used in such growth experiments include SiO_2 [7], Si_3N_4 [8, 9] and graphite [10–12]. In the case of graphite, a lot of experimental and simulation works have been done on the deposition of metals for obtaining microscopic parameters [13, 14]. Highly oriented pyrolytic graphite (HOPG) is a non-reactive substrate with a perfect atomically flat surface over dimensions of a few 100 nm. Investigation of the

growth process on HOPG reveals the interplay between the different elementary processes in initial nucleation and later growth [15].

There have been several reports on experimental studies of the surface morphology of Sb on HOPG using different *ex situ* characterization techniques such as atomic force microscopy (AFM) [16], transmission electron microscopy (TEM) [17–19], and scanning electron microscopy (SEM) [20]. Various types of structures such as fractal, flower-shaped islands as well as compact islands of Sb on graphite were observed in these studies. The mechanisms behind the formation of different types of Sb structures on graphite are difficult to be revealed from *ex situ* characterization. The film growth mechanism and surface morphology are expected to be understood in more detail by using *in situ* scanning tunnelling microscopy (STM). STM is a powerful tool that images the surface topography in real space with atomic resolution, and it is thus quite effective for studying irregular clusters and islands in the early growth stage.

Here, we report our investigations of the nucleation and growth of Sb on HOPG in ultrahigh vacuum (UHV) using *in situ* STM at room temperature (RT). We observed three types of structures, namely three-dimensional (3D), 2D and 1D crystalline islands on HOPG. The shape and size of the islands depend on a variety of growth parameters, i.e. flux and deposition time. Most of the nucleation and growth of spherical 3D islands occurs at low flux and RT. With a moderate flux, all three types of structure grow initially, but further deposition leads to mostly 2D and 1D crystalline islands at RT. The main focus of this paper is to identify the detailed atomic structures of these three different types of Sb nanostructure on HOPG. We found that the 3D and 2D Sb structures have basically the same crystalline structure as the bulk, but the 1D structure shows a significant deviation from the bulk Sb lattice. The formation of 3D, 2D and 1D islands offers great potential to prepare nanostructures for different functions.

2. Experimental details

The experiments were conducted in an Omicron UHV system (base pressure $\sim 1 \times 10^{-10}$ mbar) equipped with STM and Aüger electron spectroscopy. After cleaving in air, the HOPG substrate was transferred into the chamber immediately and degassed at $\sim$800 K for a few hours before using. In our experiments, the Sb flux was produced from a W-boat evaporator in the temperature range 600–700 K measured using a chromel–alumel thermocouple. For source temperatures less than 800 K, Sb mostly evaporates as Sb_4. The Sb_2 and Sb_1 vapour pressure in this temperature range can be neglected because they are about two orders of magnitude less than that of Sb_4 [21]. Before deposition, the Sb source was extensively degassed at 550 K in order to remove contamination. The flux was calibrated by measuring the volume of Sb islands on HOPG in STM images (assuming a sticking probability near 1). The deposition amount and coverage are measured in units of monolayer (ML). 1 ML is equivalent to an atomic density of 1.0×10^{15} cm^{-2}, which is the number of atoms in a sheet of thickness 3.1 Å (the average bond distance in α-Sb) in bulk density. In the results presented here, the sample was kept at RT during deposition and STM measurements. Additional x-ray photoemission spectroscopy measurements indicated no interaction or intermixing between Sb and graphite. After Sb deposition on HOPG with different fluxes and/or deposition times, samples were transferred to the STM stage without breaking the vacuum. All STM images were acquired in constant current mode with electrochemically etched tungsten tips. Typical sample biases ranging from $+0.3$ to $+0.7$ V, and tunnelling currents between 0.2 and 0.6 nA were used. The finite tip size and multiple-tip effects often make the 3D islands appear bigger than their real size, and generate artefacts in the STM images. Great care was taken in our experiments to minimize these effects.

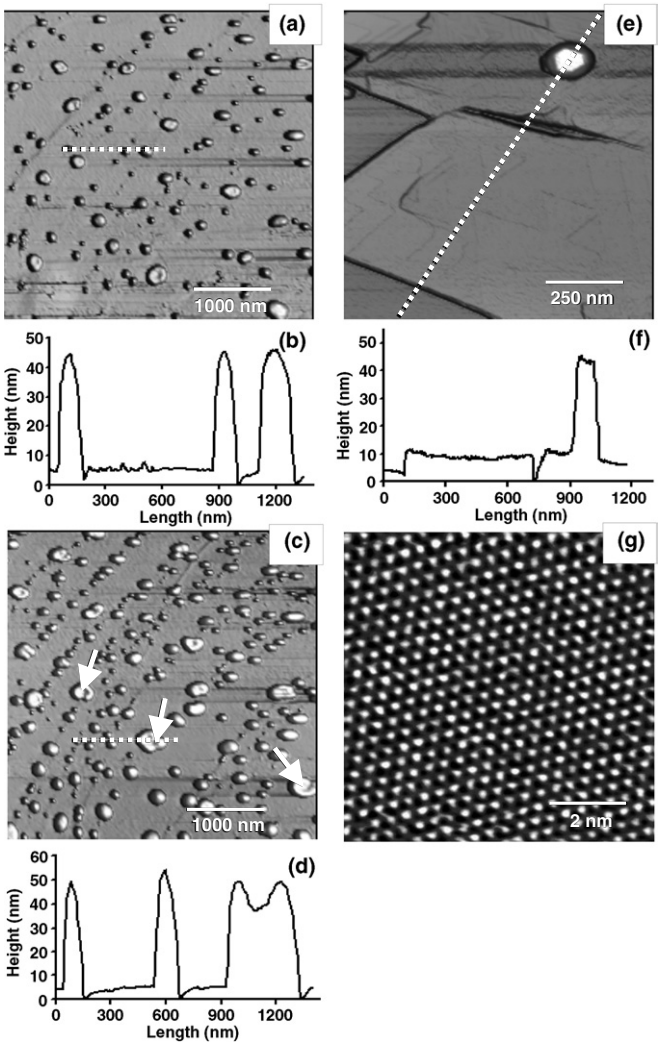

Figure 1. (a) 3D-view STM image after 2.9 ML Sb deposition on HOPG surface at RT with a flux of 1.8 Å min^{-1}; (b) height profile along the dotted line indicated in (a). (c) STM image of HOPG surface after 5.8 ML Sb deposition at a rate of 1.8 Å min^{-1}; the arrows indicate coalescence islands; (d) height profile across 3D islands along the dotted line in (c). (e) 3D-view STM image of a 1 μm × 1 μm area of HOPG after 31 ML Sb deposition at RT with a flux of 4 Å min^{-1}; (f) height profile along the dotted line scan in (e). (g) Small-area (8 nm × 8 nm) image taken on the top region of 3D island. In figure (g), the imaging conditions are: $V_s = +0.63$ V, $I_t = 0.6$ nA, and a 2D Fourier transform filter has been applied in order to minimize noise.

3. Results and discussion

3.1. Amorphous and crystalline 3D island formation

After depositing ∼2.9 ML Sb on a clean surface of HOPG at low flux (∼1.8 Å min^{-1}) at RT, we obtained only spherical 3D islands located mostly along step edges, as shown in figure 1(a). The compact spherical shape of these 3D islands is thermodynamically most favourable, and indicates a sufficiently high mobility at the island edges. These islands were

formed by diffusion and coalescence of Sb_4 on the graphite surface, in agreement with previous investigations of Sb_4 mobility and aggregation on HOPG [18, 19]. We observed a broad size distribution of 3D Sb islands on the graphite surface. A cross-section of 3D islands shown in figure 1(a) is given in figure 1(b). The average height of these 3D islands is 41 ± 5 nm and the lateral size is in the range 70–300 nm. After 5.8 ML deposition at the same rate, we obtained more islands with increased average heights (52 ± 5 nm) and lateral size range from 70 to 380 nm, as shown in figure 1(c). This indicates that newly deposited molecules join existing islands as well as forming new islands. Line profiles indicate that some large islands are formed by the coalescence of a few smaller ones, such as those pointed out by the arrows in figure 1(c). Figure 1(d) displays the cross-section profile of one of such island as well as some small islands nearby. We have not observed any facet formation and ordered atomic structures on these 3D islands at low deposition amounts. STM normally cannot resolve internal features of an object directly. Thus we are not able to verify whether these 3D islands are amorphous or crystalline. Previously, TEM investigations by Stegemann *et al* [22] showed that 3D spherical Sb nanoparticles are amorphous whereas fingerlike particles are crystalline. The parallel TEM and STM investigations of Sb particles on graphite obtained in cluster-beam deposition also showed that they are amorphous [23]. These observations indicate that the smooth-curved 3D islands are most likely amorphous in nature.

Increasing the deposition amount of Sb leads to a change in the surface morphology of the 3D islands. In addition, 2D and 1D islands start forming. After 31 ML Sb deposition on HOPG at a flux of ∼4 Å min^{-1} at RT, we obtained a faceted 3D island, which indicates a crystalline structure inside, together with crystalline 2D islands, as shown in figure 1(e). Some surface area, such as that near the lower left corner of figure 1(e), remains the bare HOPG substrate. In the next section, we will give more details about the formation of the crystalline 2D islands of Sb. The lateral size and height of the 3D island in figure 1(e) are ∼150 nm and ∼45 nm from graphite surface, respectively, as shown in figure 1(f). Also the cross-section of the top of the 3D island shows a smooth profile, indicating a crystalline structure inside. The hexagonal facet observed on top of this 3D island is similar to those observed by Kaiser *et al* using SEM [20]. Further zoom-in scans on the flat top facet of the 3D island reveal a hexagonal ordered structure, as shown in figure 1(g), with a lateral period 4.28 ± 0.05 Å. Comparing with the lattice parameters of α-Sb(111) [24], our measured lateral period agrees well with the expected lateral period (4.31 Å). From these experimental observations, it is confirmed that these 3D islands have crystalline structure and the phase transition from amorphous to crystalline depends on adequate deposition amount. Similar results were also observed by Savage and Lagally [25] in the case of Sb on GaAs. In their reflection high-energy electron diffraction studies, an amorphous to crystalline phase transition of Sb occurs on GaAs(110) after a deposition of 20 ML Sb at RT. In the case of Sb on HOPG, Stegemann *et al* [22] also found that the phase transition from amorphous to crystalline occurs at 40 ML Sb deposition on HOPG.

The dependence of the number density of 3D islands on coverage of Sb on HOPG at a flux of 1.8 Å min^{-1} is depicted in figure 2(a). The density peaked at $\sim 1.7 \times 10^9$ cm^{-2} after 5.8 ML Sb deposition. With more Sb deposition, the island density decreased and reached $\sim 1.3 \times 10^9$ cm^{-2} after 14.5 ML Sb deposition on HOPG. This indicates that at the initial stage of deposition, the density of 3D islands increases due to the dominance of the nucleation process. With further deposition, the coalescence process coexists with nucleation and growth, and later dominates over the nucleation process. We also performed experiments at different fluxes to obtain further details about the variation of number density of 3D islands. It was observed that the number density of 3D islands at a flux of 4 Å min^{-1} is less than that at a flux of 1.8 Å min^{-1} with nearly the same deposition amount. We observed some big and

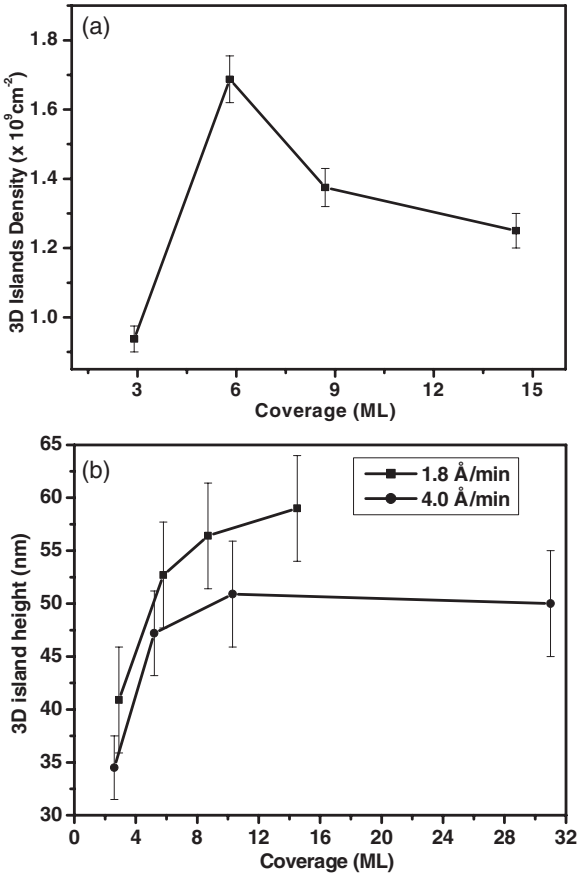

Figure 2. (a) Evolution of 3D island density as a function of coverage at a flux of 1.8 Å min^{-1}; (b) variation of 3D island average height with coverage of Sb at different fluxes.

distorted spherical 3D islands (pointed out by the arrows in figure 1(c)); they were formed by the coalescence of smaller spherical islands. The decrease of 3D island number density is due to the formation of 2D and 1D structures later on besides the coalescence of 3D islands. With a comparative deposition flux, Kaiser *et al* [20] observed dendritic structures due to aggregation and insufficient coalescence of Sb clusters and small 3D islands, whereas no such types of structure were observed in our repeated runs. This could be due to different step densities on the HOPG used. In [20, 22], the step spacing is at least a few μm, and there is often no step in an area of several μm^2 where dendritic islands form. On our HOPG samples, the step spacing is mostly less than 1 μm, so the steps act as nucleation/trapping sites for compact 3D islands. Yoon *et al* [18] showed that intermediate-size Sb clusters (Sb_n with $n \sim 90$–500) deposited on low-defect-density HOPG form extended ramified islands, whereas relatively compact islands are formed on samples with relative high defect density. The extremely low step density may lead to the accumulation of intermediate-size Sb clusters to a sufficient density, and the aggregation and partial coalescence of these Sb clusters result in the dendritic structures.

The variation of the average height of 3D islands as a function of coverage of Sb on HOPG at different fluxes is plotted in figure 2(b). At a flux of 4 Å min^{-1}, the 3D island height increases with deposition time initially and later saturates at 50 ± 5 nm. This is because, after the initial

stage, the nucleation and growth of 3D islands are suppressed due to the effective growth of 2D and 1D islands. At a lower flux ($\sim$1.8 Å min^{-1}), initially the height of the islands increases quickly and later it increases slowly with deposition amount. The average height of 3D islands after 14.5 ML Sb deposition at a flux of $\sim$1.8 Å min^{-1} is 59 $\pm$ 5 nm, whereas at a flux of 4 Å min^{-1}, the average height of islands saturates at 50 $\pm$ 5 nm after 31 ML Sb deposition, as plotted in figure 2(b). From this observation, it is confirmed that the growth of 3D islands is favoured at a low flux.

3.2. Crystalline 2D island formation

In figure 1(e), we observed 2D island formation in addition to one 3D island on a 1 μm^2 area of HOPG after 31 ML Sb deposition at a rate of $\sim$4 Å min^{-1} at RT. Most wetting-layer-like triangular 2D islands have thickness $\geqslant$6.5 nm. It is highly desirable to find conditions to preferably grow nanostructures of one type and suppress others. Figure 3(a) displays an STM image taken on an HOPG sample after 130 ML deposition of Sb at a high flux ($\sim$20 Å min^{-1}) at RT. In this condition, only multilayer 2D islands were observed on the 1 μm $\times$ 1 μm area of HOPG. Comparing figures 1(e) and 3(a), it is confirmed that the higher flux is more favourable for 2D structures rather than 3D structures. A zoom-in scan on the 2D islands reveals atomic steps, as shown in figure 3(b). The average height of atomic steps is 3.85 $\pm$ 0.35 Å. A further zoom-in scan on the flat terrace reveals a hexagonal ordered structure of Sb, as shown in figure 3(c), with a period 4.22 $\pm$ 0.16 Å. Within experimental uncertainty, our measured step height and lateral period values agree with the bulk α-Sb(111) values [24] of step height (3.76 Å) and lateral period (4.31 Å).

3.3. Crystalline nanorod formation

Figure 4(a) displays an STM image taken on a HOPG sample after 3.9 ML Sb deposition with a flux of 4 Å min^{-1} at RT. In addition to the 3D and 2D islands, we see a 1D nanorod with height of about 22 nm and width of $\sim$35 nm in the upper part of figure 4(a) as shown in the line profile in figure 4(b). Besides this relative long Sb nanorod, there are two short rods near a 3D island in the lower half of the image. The heights of these rods are about 13 nm. After depositing 14.5 ML Sb at RT, we obtained bundles of 1D nanorods with width of $\sim$15 $\pm$ 4 nm as shown in figure 4(c). These rods are folded by nearly 90°. We have observed bundles of nanorods on several samples which were prepared at moderate high flux or after a large amount of Sb deposition. Only at the initial stage of growth were individual nanorods observed on the bare graphite surface. The lengths of nanorods are from a few 100 nm to more than 1 μm. Our results also indicate that the Sb rods are not necessarily formed along step edges of HOPG surface.

Figure 4(d) displays an STM image of a scan area (9 nm^2) taken on top of the turning corner of Sb nanorods, showing atomic steps and lateral periodic structures. After measuring on many steps we got an average step height of 2.97 $\pm$ 0.31 Å on 1D structures. Figure 4(d) reveals a square ordered structure with a period of 4.15 $\pm$ 0.11 Å on the nanorod. These 1D structures show a different crystal structure than the bulk α-Sb. Although the exact growth mechanism of this quasi-1D Sb structure and its crystalline structure are not very clear, it is an allotropic modification of Sb on graphite at the nanometre scale. It is well known that group V elements show rich allotropic transformation with changing temperature and/or pressure [26, 27]. Recently, some reports [28, 29] have described a new allotrope of these group V elements by tuning the thickness of the film at the nanometre scale. Bernhardt *et al* studied the allotropic modification of Sb_4 molecules in thin films and obtained nearly cubic

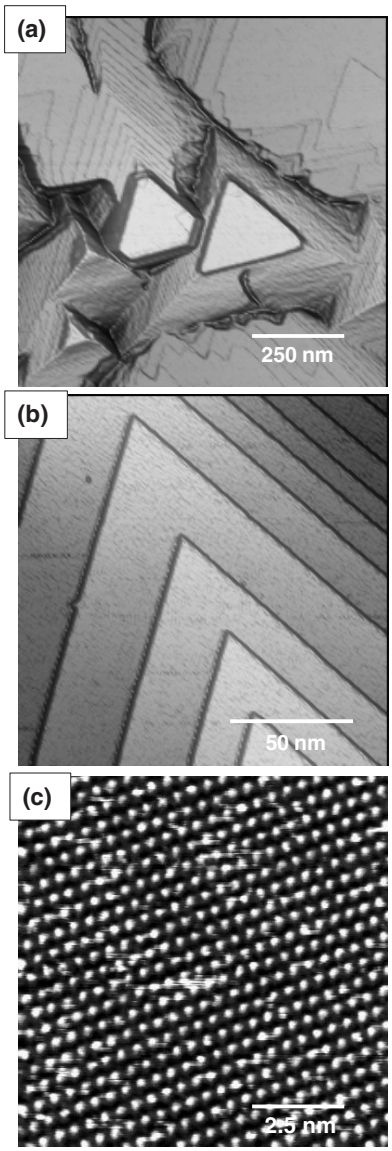

Figure 3. 3D-view STM images of 130 ML Sb deposited HOPG at RT with a flux of ∼20 Å min^{-1}. Scan sizes are (a) $(1000\ \text{nm})^2$; (b) $(150\ \text{nm})^2$. (c) Small-area (10 nm × 10 nm) image taken on the top region of a 2D island. In figure (c), a 2D Fourier transform filter has been applied in order to enhance the well-ordered structure. Imaging conditions for figure (c): $V_s = +0.63$ V, $I_t = 0.6$ nA.

lattice structure instead of rhombohedral Sb on $MoS_2(0001)$ and $AuSb_2(001)$ [28]. Nagao *et al* [29] also found that an ultrathin film of Bi on Si(111) shows an allotropic transformation as a function of thickness in the range of several atomic layers.

Our proposed model for the crystal structure of 1D Sb islands is shown in figure 5. Here we considered the simple cubic (sc) structure of 1D Sb nanorods with lattice constant $a_{\text{cub}} = 2.98$ Å based on the result of Vereshchagin *et al* [30]. They reported a phase transition of Sb from rhombohedral to sc under high pressure, and found an sc lattice constant of 2.98 Å,

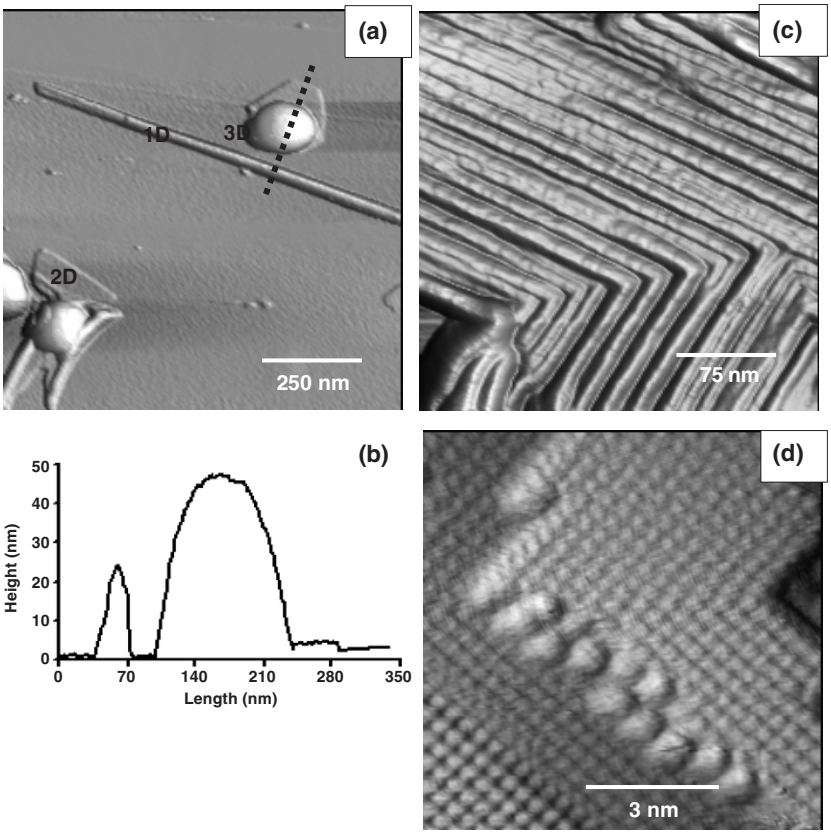

Figure 4. (a) 3D-view STM image after 3.9 ML Sb deposition on HOPG with a flux of 4 Å min^{-1} at RT. Scan size: $(1000\ \text{nm})^2$; (b) line profile across 1D, 3D and 2D structures as indicated by dotted line in (a). (c) 3D-view STM image with scan area 300 nm × 300 nm of HOPG surface after 14.5 ML Sb deposition at RT; (d) small-area (9 nm × 9 nm) image taken on the top region of a 1D structure. Imaging conditions: $V_s = +0.63$ V, $I_t = 0.6$ nA.

slightly larger than the Sb–Sb bond length (2.91 Å). The step height (2.97 ± 0.31 Å) of the observed 1D Sb structure is approximately equal to the distance between two neighbouring (100) lattice planes (2.98 Å) of the sc structure. Figure 5 shows the (100) surface of the sc lattice with the dashed-line square representing a $(\sqrt{2}\times\sqrt{2})$ R45° cell. Our experimental lattice period of 4.15 ± 0.11 Å is consistent with the proposed model lattice period ($\sqrt{2} \times 2.98$ Å $= 4.21$ Å). There should be another atom at the centre of the unit cell. In our STM image, the centre atom is invisible. In a previous study of ultrathin Bi film on Si(111) [29], one atom in the unit cell on the rhombohedral (110) face, which is the pseudo-cubic (100) face, is also invisible in the STM images and this is explained on the basis of a puckered layer structure in which the centre atom could recede by 0.5 Å. Since Sb and Bi are both group V elements with similar lattice relaxation behaviour, it is not surprising that they show the same phenomena.

Chang and Cohen [27] studied the structural stability of the rhombohedral and sc phases for the group V elements. They predicted an atomic volume 0.86 V_0 for the sc phase of Sb under high pressure, where $V_0 = 30.21$ Å^3 [24] is the atomic volume at normal pressure. In our model, the atomic volume of the sc structure is $V = 26.46$ Å^3. The ratio $V/V_0 = 0.88$ is in fairly good agreement with the predicted value of 0.86.

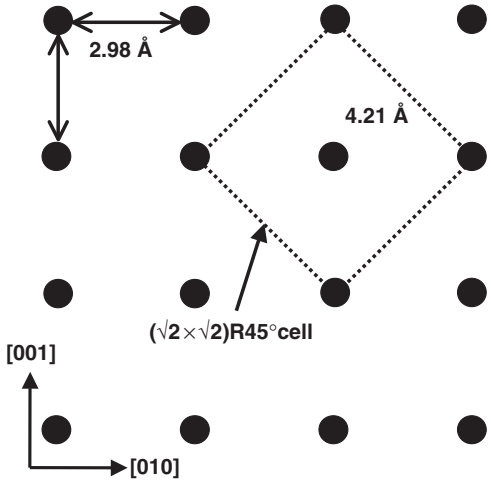

Figure 5. 2D representation of (100) sc crystal structure with lattice period ($a_{cub} = 2.98$ Å) based on [30]. Dashed lines describe a ($\sqrt{2} \times \sqrt{2}$) R45° cell.

Previously, some reports [30, 31] have described the phase transition of Sb from rhombohedral structure to cubic structure after applying a pressure ∼5–7 GPa. The phase transition in the case of the 1D structure can be explained in terms of surface stress induced pressure during nucleation. Based on nanothermodynamics [32], the surface stress induces an additional pressure ΔP in the nucleus with $\Delta P = 2\sigma/r$, which is known as Laplace–Young equation. In this equation, σ and r are the surface stress and the radius of nucleus, respectively. If we consider $\sigma \sim 0.6$ J m^{-2} (approximately the surface energy of Sb [33]) and $r \sim 1$ nm then the induced additional pressure is ∼1.2 GPa, which is a quite high pressure that could favour the sc phase. However, to fully understand the formation of a 1D structure of different phase, further theoretical modelling and calculations are needed.

4. Conclusion

In summary, we have investigated different morphologies exhibited by Sb on HOPG at RT in UHV using *in situ* STM. Various kinds of shapes and sizes of Sb islands like spherical and triangular islands were observed. Most nucleation and growth of spherical 3D islands occurs at low flux and RT. In the initial stage, amorphous 3D islands were observed on the graphite surface. As the deposition increases, crystalline 3D islands are obtained even at RT. With a moderate flux, three types of structures grow initially but further deposition leads to mostly 2D and 1D crystalline islands at RT. The detailed atomic structures of these three different types of Sb islands on HOPG have been measured. The 3D and 2D structures of Sb on graphite have the same bulk rhombohedral structure, but the 1D structure shows a sc crystalline structure. This system offers the possibility to obtain different types of nanostructures by selecting proper growth conditions like flux and exposure time.

Acknowledgments

This work was partially supported by research grants from the National University of Singapore (Grant R-398-000-008-112) and the Science and Engineering Research Council of Singapore (Grant R-144-000-088-305).

References

[1] Mo Y-W, Savage D E, Swartzentruber B S and Lagally M G 1990 *Phys. Rev. Lett.* **65** 1020
[2] Voigtlander B, Weber T, Smilauer P and Wolf D E 1997 *Phys. Rev. Lett.* **78** 2164
[3] Henry C R 1998 *Surf. Sci. Rep.* **31** 231
[4] Freund H-J 2002 *Surf. Sci.* **500** 271
[5] Yoffe A D 2001 *Adv. Phys.* **50** 1
[6] Ross C A 2001 *Annu. Rev. Mater. Sci.* **31** 203
[7] Nicotra G, Puglisi R A, Lombardo S, Spinella C, Vulpio M, Ammendola G, Bileci M and Gerardi C 2004 *J. Appl. Phys.* **95** 2049
[8] Wang L, Hu Y, Li Z, Tang J-C and Wang X-S 2002 *Nanotechnology* **13** 714
[9] Gwo S, Chou C-P, Wu C-L, Ye Y-J, Tsai S-J, Lin W-C and Lin M T 2003 *Phys. Rev. Lett.* **90** 185506
[10] Brechignac C, Cahuzac P, Carlier F, Colliex C, Leroux J, Masson A, Yoon B and Landman U 2002 *Phys. Rev. Lett.* **88** 196103
[11] Couillard M, Pratontep S and Palmer R E 2003 *Appl. Phys. Lett.* **82** 2595
[12] Marsen B and Sattler K 1999 *Phys. Rev.* B **60** 11593
[13] Lewis L J, Jensen P, Combe N and Barrat J-L 2000 *Phys. Rev.* B **61** 16084
[14] Luedtke W D and Landman U 1999 *Phys. Rev. Lett.* **82** 3835
[15] Jensen P 1999 *Rev. Mod. Phys.* **71** 1695
[16] Heyde M, Cappella B, Sturm H, Ritter C and Rademann K 2001 *Surf. Sci.* **476** 54
[17] Bardotti L, Jensen P, Hoareau A, Treilleux M, Cabaud B, Parez A and Aires F C S 1996 *Surf. Sci.* **367** 276
[18] Yoon B, Akulin V M, Cahuzac P, Carlier F, Frutos M, Masson A, Mory C, Colliex C and Brechignac C 1999 *Surf. Sci.* **443** 76
[19] Melinon P, Jensen P, Hu J X, Hoareau A, Cabaud B, Treilleux M and Guillot D 1991 *Phys. Rev.* B **44** 12562
[20] Kaiser B, Stegemann B, Kaukel H and Rademann K 2002 *Surf. Sci.* **496** L18
[21] Barnet S A, Winters H F and Greene J E 1986 *Surf. Sci.* **165** 303
[22] Stegemann B, Ritter C, Kaiser B and Rademann K 2004 *J. Phys. Chem.* B **108** 14292
[23] Villenueuve de C H, Porte L, Bardotti L, Cabaud B, Hoareau A and Treilleux M 1993 *Microsc. Microanal. Microstruct.* **4** 471
[24] Donohue J 1974 *The Structures of the Elements* (New York: Wiley)
[25] Savage D E and Lagally M G 1987 *Appl. Phys. Lett.* **50** 1719
[26] Iwasaki H and Kikegawa T 1997 *Acta Crystallogr.* B **53** 353
[27] Chang K J and Cohen M L 1986 *Phys. Rev.* B **33** 7371
[28] Bernhardt T M, Stegemann B, Kaiser B and Rademann K 2003 *Angew. Chem. Int. Edn* **42** 199
[29] Nagao T, Sadowski J T, Saito M, Yaginuma S, Fujikawa Y, Kogure T, Ohno T, Hasegawa Y, Hasegawa S and Sakurai T 2004 *Phys. Rev. Lett.* **93** 105501
[30] Vereshchagin L F and Kabalkina S S 1965 *Sov. Phys.—JETP* **20** 274
[31] Kolobyanina T N, Kabalkina S S, Vereshchagin L F and Fedina L V 1969 *Sov. Phys.—JETP* **28** 88
[32] Wang C X and Yang G W 2005 *Mater. Sci. Eng.* R **49** 157
[33] Jiang Q, Lu H M and Zhao M 2004 *J. Phys.: Condens. Matter* **16** 521